Hindawi

Research Article

Effects of In-Situ Drying–Wetting Cycles on the Stress-Dependent Water Retention Behavior of Intact Loess

X. M. Li,[1] S. J. Di,[2] L. Shi,[2] Y. Zhang,[2] P. Huang,[2] and Q. Y. Mu [3]

[1]*Xi'an Siyuan University, Xi'an, China*
[2]*Northwest Engineering Corporation Limited, Power China, Xi'an, China*
[3]*Department of Civil Engineering, Xi'an Jiaotong University, Xi'an, China*

Correspondence should be addressed to Q. Y. Mu; 445953087@qq.com

Understanding the effects of in-situ drying–wetting pattern on the stress-dependent water retention curve of intact loess is vital for addressing geotechnical problems in loess regions. The principal objective of this study is to investigate the influence of in-situ drying–wetting on the stress-dependent water retention behavior of intact loess. To meet this objective, six drying–wetting tests were carried out using a suction- and stress-controlled pressure plate extractor. Intact loess was sampled from three different depths: 1.0, 3.0, and 5.0 m. For specimens from each depth, two vertical net stresses (i.e., 0 and 50 kPa) were applied prior to the drying–wetting cycle. Experimental results revealed that the in-situ drying–wetting pattern greatly affected various aspects of the water retention behavior, particularly the hysteresis. The hysteresis of the specimen from 5.0 m is about 82% and 77% larger than that of the specimens from 1.0 and 3.0 m, respectively. This is because the specimen from 5.0 m has some large-size pores (i.e., $>400\,\mu$m), which were not found in specimens from 1.0 and 3.0 m. These large-size pores enhance pore nonuniformity and hence the hysteresis. Furthermore, specimens from different depths consistently showed a reduction of hysteresis when the stress was increased from 0 to 50 kPa. The reduction is the most significant for a specimen from 5.0 m due to the collapse of large-size pores under compression.

1. Introduction

Understanding the stress-dependent water retention curve (WRC) of intact loess is essential for addressing many geotechnical problems in loess regions, such as rainfall-induced excessive embankment settlement [1–3], failure of landfill cover system [4–6] and slope instability [7, 8]. Thus, some experimental studies have been carried out in this area. Muñoz-Castelblanco et al. [9] measured the WRC of an intact loess. The WRC showed a peculiar shape, with negligible hysteresis around the initial suction and marked hysteresis at lower and higher suctions. The zone having the smallest hysteresis was corresponding to natural variations of water content in the field. Ng et al. [10] compared the WRC of intact and compacted loess. The former had a larger hysteresis than the latter, particularly at suctions below 20 kPa, mainly because of ink-bottle effects induced by extra-large pores in the intact loess. Recently, Mu et al. [11]

studied the WRCs of intact, compacted, and reconstituted loess specimens subjected to two drying–wetting cycles. The air entry value (AEV) and hysteresis of all specimens consistently changed with increasing drying–wetting cycles. It should be pointed out that each of the previous studies used intact specimens from a single depth. Soils at various depths are expected to have different WRCs because they have been subjected to different in-situ drying–wetting cycles and therefore own different pore structures [12–14]. So far, the effects of in-situ drying–wetting on the water retention behavior of unsaturated intact loess have not been purposely studied, in spite of some previous studies of unsaturated loess in the literature.

This study aims to investigate the effects of in-situ drying–wetting cycles on the stress-dependent WRC of an intact loess. WRCs of intact loess retrieved at 1.0, 3.0, and 5.0 m depths were measured using a pressure plate extractor. For soil from each depth, vertical net stresses of 0–50 kPa

were applied. In addition, mercury intrusion porosimeter (MIP) and X-ray diffraction (XRD) tests were carried out to measure the pore size distribution (PSD) and mineral composition of the tested soil, respectively.

2. Test Program and Test Apparatus

Six drying and wetting tests were carried out to study the water retention behavior of an intact loess (i.e., D1S0, D1S50, D3S0, D3S50, D5S0, and D5S50). Soil samples were obtained from three different depths (i.e., 1.0, 3.0, and 5.0 m), and each of them was tested at two vertical net stresses (i.e., 0–50 kPa). It should be pointed out that the vertical net stress of 50 kPa is close to the in-situ stress state and related to many geotechnical problems, such as subgrade settlement and shallow slope failure [4, 8]. Comparisons of the obtained six WRCs would reveal the influence of drying–wetting and stress on the water retention behavior.

In addition, to interpret the previous water retention behavior, a series of XRD and MIP tests were carried out to investigate the mineral composition and PSD of loess samples from 1.0, 3.0, and 5.0 m depths at their in-situ states, respectively.

The tests were conducted using a suction and stress-controlled pressure plate extractor [15]. The suction, which equals the difference between pore air pressure and pore water pressure, was controlled by the axis translation technique. The vertical net stress was imposed using a loading rod. A dial gauge was attached to the loading rod to monitor soil volume change. In addition, the outflow/inflow rate of soil water during the drying/wetting process was measured through a ballast tube. Details of the apparatus were given by Ng and Pang [15].

3. Test Soil

Three loess blocks (about $250 \times 250 \times 250$ mm in dimension) were sampled at 1.0, 3.0, and 5.0 m depths in Yan'an, China. The particle size distributions are measured in accordance with [16] and shown in Figure 1(a). The samples from different depths show similar particle size distributions, with clay (i.e., <0.005 mm) and silt (i.e., 0.005–0.074 mm) fractions varying from 14.0% to 17.7% and from 78.2% to 82.2%, respectively. The liquid limits, which are measured following [17], are 30.3%, 30.7%, and 31.5% for samples from 1.0, 3.0, and 5.0 m, respectively. Similarly, the differences in plastic limit are also negligible (i.e., less than 1%).

The XRD patterns of these three samples are shown in Figure 1(b). Similar peak positions and peak densities are observed for those XRD patterns. The mineralogical compositions of tested loess are determined based on the XRD patterns and shown in Table 1. For the intact loess from 1.0 m, the nonclay minerals, including quartz, albite, and calcite, are identified, while the clay minerals mainly consist of nimite and muscovite. Calcite is a cementitious material that is probably acquired from reprecipitation [18]. In addition, the intact loess from 3.0 to 5.0 m contains the same minerals to that from 1.0 m due to their similar XRD patterns.

Soil water contents at the sampling locations were monitored from April to November in 2018 using the time domain reflectometry [19, 20] and shown in Figure 2. This period covers both the dry and wet seasons in Yan'an. The measured results are, therefore, representative of the variations of soil water content in the field. During this period, the intact loess at 1.0 and 3.0 m depths experienced two drying and wetting cycles, corresponding to changes in the degree of saturation from 32% to 96%. In contrast, soil water contents at 5.0 m depth remained almost constant throughout the monitoring period.

4. Specimen Preparation and Test Procedures

Specimens were extracted from the loess blocks using an oedometer ring (61.8 mm in diameter and 19 mm in height). The specimen surface was carefully smoothed with a wire saw. The dry density and gravimetric water content of each specimen were measured and summarized in Table 2. In addition, the initial suction was measured through the null-type axis translation technique [21]: 88, 34, and 32 kPa for the specimens from 1.0, 3.0, and 5.0 m, respectively.

For XRD tests, the loess sample was ground using a McCrone Micronising mill for 20 min to obtain powder specimens [18]. The random powders were prepared through a razor-tamped surface method [22]. For MIP tests, small cubes with dimensions of approximately $5.0 \times 5.0 \times 5.0$ mm were carefully cut from loess blocks. The prepared cuboid specimens were dehydrated by freeze–drying method to protect the structure [23].

The prepared specimens were then set up in the pressure plate extractor. The predefined vertical net stress (i.e., 0 and 50 kPa) was applied to each specimen at the constant water content condition. After that, all specimens were wetted to 0.1 kPa in steps. At each step, soil suction was controlled using the axis-translation technique, as discussed earlier. About 1–2 weeks were required to reach the equilibrium condition, in which the change in water content was less than 0.04%/day [24]. The soil volumetric water content was calculated according to the recorded vertical displacement and water content. In a similar approach, all specimens were dried to 400 kPa and finally rewetted to the initial suction in steps.

For XRD tests, diffraction patterns were obtained through the PANalytical X'Pert Pro diffractometer, with Cu Kα ($\lambda = 1.5418$ Å) radiation generated at 44 kV and 40 mA. The specimens were scanned from 2° to 45° with a rate of 1° 2θ/min. The PSDs were measured through the Micromeritics Auto Pore IV 9500 V1.04. The applied pressure ranged from 0.5 to 413,685 kPa, corresponding to intrusion pore diameters from 0.003 to 360 μm.

5. Interpretations of Experimental Results

5.1. Pore Size Distribution. Figure 3(a) shows the MIP results of tested specimens at the in-situ stress state. The intruded void ratios and the actual void ratios calculated from the mass-volume relationship are labeled by i and c, respectively. The intruded void ratios are 0.75, 0.72, and 0.69 for
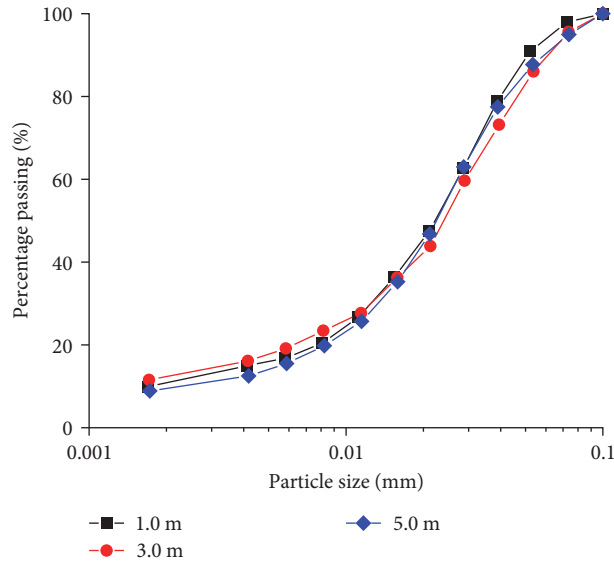
(a)
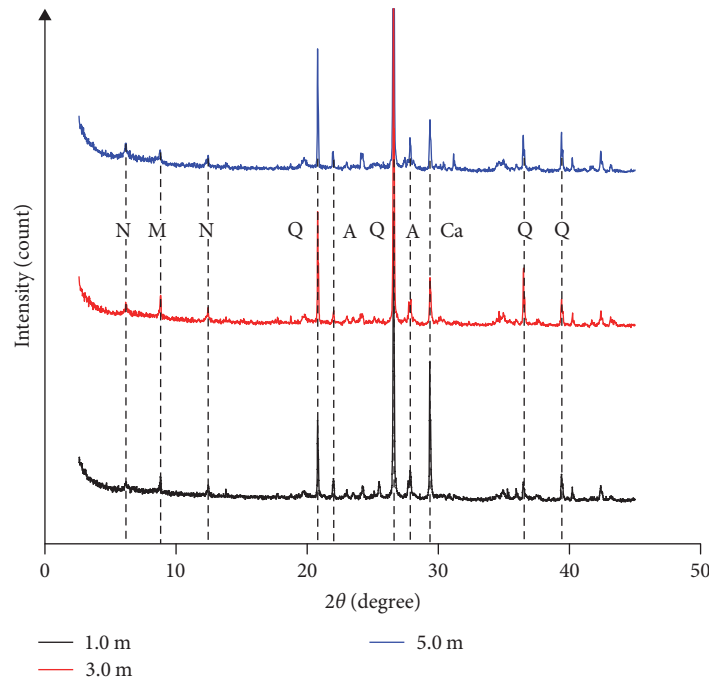
(b)

Figure 1: Properties of tested intact loess: (a) particle size distribution; (b) X-ray diffraction pattern (Q, quartz; A, albite; Ca, calcite; M, muscovite; N, nimite).

Table 1: Mineralogical compositions of intact loess from different depths.

Test soil (m)	Nonclay minerals			Clay minerals	
1.0					
3.0	Calcite	Albite	Quartz	Nimite	Muscovite
5.0					

specimens from 1.0, 3.0, and 5.0 m, respectively. Compared with the actual void ratios calculated from the mass–volume relationship, the nonintruded void ratios are almost negligible (i.e., less than 0.02) for specimens from 1.0 and 3.0 m. In contrast, the specimen from 5.0 m has a nonintruded void ratio of 0.09, corresponding to about 11.5% of its total pore volume. The nonintruded void ratio is attributed to the limitation of MIP device, which is unable to determine large-size
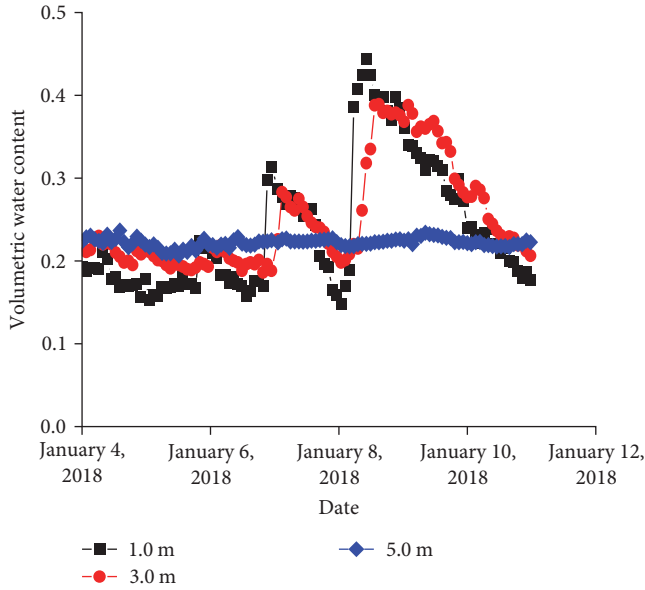
FIGURE 2: Field monitoring of changes in soil volumetric water content with time at 1.0, 3.0, and 5.0 m depths.

TABLE 2: Physical and index properties of loess.

Parameter		Value	
Sampling depth (m)	1.0	3.0	5.0
Dry density, ρ_d (g/cm^3)	1.52	1.56	1.51
Initial gravimetric water content, w (%)	12.74	14.37	15.08
Initial suction, s (kPa)	88	34	32
Specific gravity, d_s	2.69	2.69	2.69
Calculated void ratio from mass–volume relationship, e_0	0.77	0.72	0.78
Intruded void ratio, e_i	0.75	0.72	0.69
Liquid limit, w_L (%)	30.3	30.7	31.5
Plastic limit, w_p (%)	12.5	12.1	12.9
Plasticity index, I_p (%)	17.8	18.6	18.6
Unified soil classification (ASTM D2487)		CL	

pores larger than $400\,\mu m$ and small-size pores smaller than $0.007\,\mu m$ [25]. According to the study of Ng et al. [10], the nonintruded pores of intact loess are mostly large-size pores because intact loess does not have many pores smaller than $0.007\,\mu m$. The large-size pores are not found in the intact loess from 1.0 and 3.0 m, probably because they have collapsed due to the numerous drying and wetting cycles in the field (see Figure 2). They are preserved in the specimen from 5.0 m, at which soil water content remained almost constant.

Based on the results in Figure 3(a), the pore size density function is calculated and shown in Figure 3(b). The specimens from 1.0, 3.0, and 5.0 m show a similar tri-modal PSD. The dominant pore of the specimen from 3.0 m (i.e., $5.8\,\mu m$) is smaller than those of the other two specimens (i.e., $7.2\,\mu m$), mainly because it is about 3% denser (see Table 2). More importantly, it should be noted that only the specimen from 5.0 m has some nonintruded large-size pores (see

Figure 3(a)). Its pores are, therefore, the most nonuniform. The influence of pore nonuniformity on soil WRC is discussed later.

5.2. Stress-Dependent Water Retention Curve. Figure 4(a) shows WRCs of the intact loess under zero stress. For each specimen, the AEV, void ratio after drying–wetting, desorption, and adsorption rates are determined and summarized in Table 3. Along the first wetting path, the specimens D1S0 and D3S0 became almost saturated when suction was reduced to 3 kPa. The specimen D5S0 reached saturation at a much lower suction (about 0.1 kPa), mainly because it has some large-size pores (see Figure 3(a)). In addition, the adsorption rates of D1S0 (0.035 (log kPa)$^{-1}$) and D3S0 (0.034 (log kPa)$^{-1}$) are about two times that of D5S0 (0.016 (log kPa)$^{-1}$). Along the subsequent drying path, similarly, the desorption rates of D1S0 (0.034 (log kPa)$^{-1}$) and D3S0 (0.035 (log kPa)$^{-1}$) are 11.8% and 14.3% larger than that of D5S0 (0.030 (log kPa)$^{-1}$), respectively. The differences between these three specimens in terms of the adsorption and desorption rates are likely related to their PSDs. As revealed in Figure 3(a), the specimen from 5.0 m has more nonuniform PSD, which would result in smaller adsorption and desorption rates [26, 27]. As shown in Table 3, the AEV of intact loess at 3.0 m (i.e., 8.2 kPa) is larger than that of intact loess at 1.0 m (i.e., 5.7 kPa) and 5.0 m (i.e., 6.5 kPa), mainly because of the smaller void ratio owned by the former soil. Moreover, during the drying–wetting cycle, the volume changes of specimens D1S0, D3S0, and D5S0 are essentially elastic under zero stress.

Figure 4(b) shows the WRCs of the intact loess under a vertical net stress of 50 kPa. The key parameters of each WRC are also given in Table 3. It is clear that specimen D5S50 has smaller adsorption and desorption rates than D1S50 and D3S50. This is consistent with the findings from Figure 4(a), suggesting that the observed effects of sampling depth on WRC are reliable. On the other hand, when the vertical net stress was increased from 0 to 50 kPa, the AEV increased by 10.5%, 8.5%, and 18.5% for specimens from 1.0, 3.0, and 5.0 m, respectively. The increment is the highest for the specimen from 5.0 m. A similar trend can be obtained for the adsorption and desorption rates (see Table 3). More importantly, in contrast to the zero stress, the specimens D1S50, D3S50, and D5S50 contract, and hence the irreversible contraction of 3.9%, 1.4%, and 6.5% are observed during the drying–wetting cycle. These observations suggest that the specimen from 5.0 m is most sensitive to net vertical stress because its large-size pores can be readily compressed.

5.3. Degree of Hysteresis in the WRC. Figure 5 shows the relationship between suction and the degree of hysteresis. At a given suction, the degree of hysteresis is calculated by the ratio of the difference in the volumetric water contents along drying and wetting paths to their average value [28]. Parabolic shapes are observed for this relationship, with peak values appearing at a suction of 20 kPa. Under a given vertical net stress, the average degree of hysteresis of D5S0 and D5S50 (i.e., 0.226 and 0.201) is 81.4%–82.6% and 76.5%–77.6% larger than that of D1S0 and D1S50 (i.e., 0.042 and 0.035) as well as
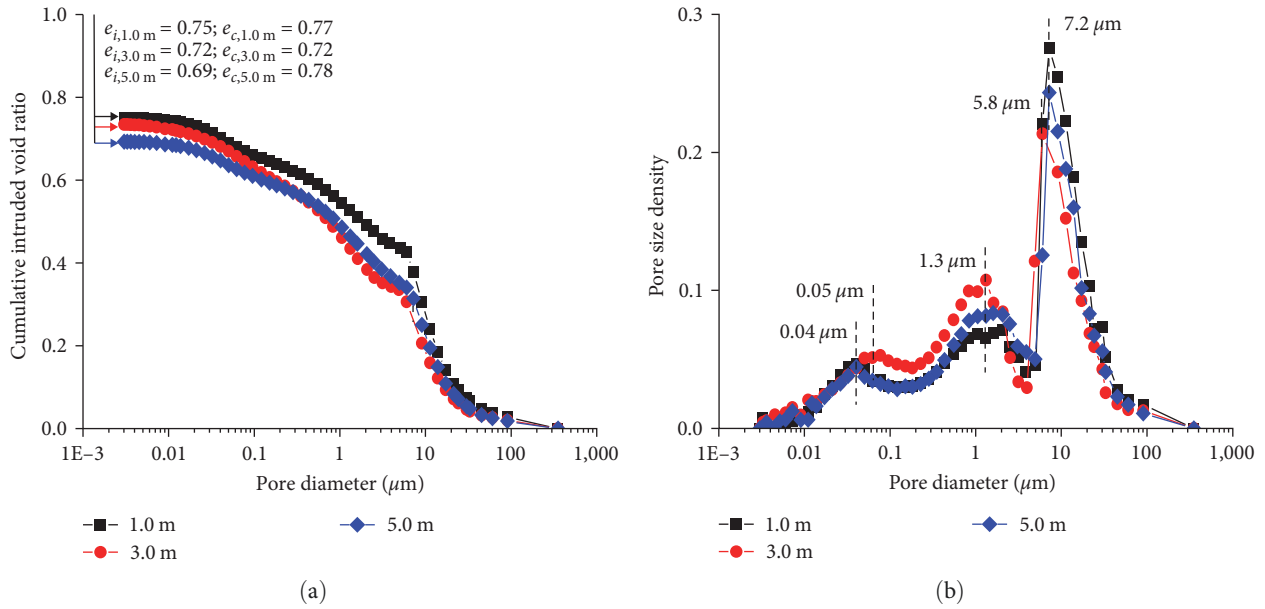
FIGURE 3: MIP results of intact loess at 1.0, 3.0, and 5.0 m depths: (a) cumulative intruded void ratio; (b) pore size density.
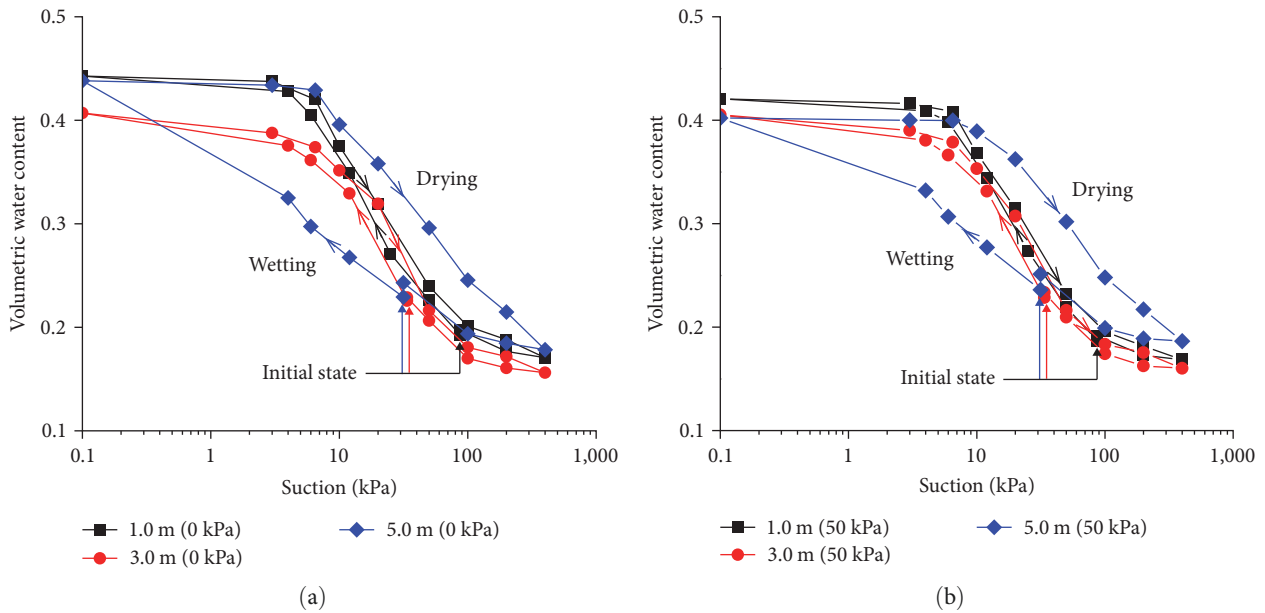

FIGURE 4: Water retention curves of intact loess at 1.0, 3.0, and 5.0 m depths: (a) vertical net stress: 0 kPa; (b) vertical net stress: 50 kPa.

D3S0 and D3S50 (i.e., 0.053 and 0.045), respectively. The significant hysteresis of the specimens from 5.0 m was likely attributed to their large-size pores. These pores enhance the pore nonuniformity and thus the ink-bottle effects, as illustrated by Ng et al. [10].

For specimens from all three depths, the degree of hysteresis consistently decreases with increasing vertical net stress. The reduction is the most obvious for the specimen from 5.0 m. This is consistent with the finding in Figure 4 and probably attributed to the collapse of large-size pores.

6. Conclusions

In situ, the intact loess from different depths has been subjected to different drying–wetting cycles, which have a significant effect on the soil structure and water retention behavior. To understand the effects of in-situ drying–wetting cycles on the stress-dependent water retention behavior of intact loess, the intact loess from different depths (i.e., 1.0, 3.0, and 5.0 m) were tested by pressure plate and microstructure tests.

TABLE 3: Parameters of WRCs for intact loess at 1.0, 3.0, and 5.0 m depths.

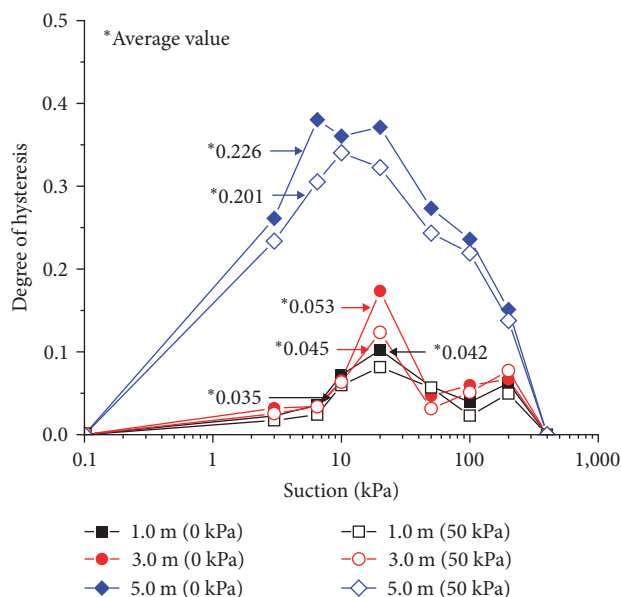| Specimen identity	Depth (m)	Vertical stress (kPa)	Air entry value (kPa)	Void ratio after drying–wetting	Desorption rate $(\log kPa)^{-1}$	Adsorption rate $(\log kPa)^{-1}$
D1S0	1.0	0	5.7	0.77	0.034	0.035
D1S50		50	6.3	0.74	0.033	0.035
D3S0	3.0	0	8.2	0.72	0.035	0.034
D3S50		50	8.9	0.71	0.033	0.035
D5S0	5.0	0	6.5	0.77	0.030	0.016
D5S50		50	7.7	0.72	0.028	0.019

FIGURE 5: Degree of hysteresis of tested intact loess.

The intact loess sampled from 1.0 and 3.0 m depths showed almost identical hysteresis, desorption, and adsorption rates. When the sampling depth was increased to 5.0 m, the desorption and adsorption rates decreased by about 14% and 54%, respectively, and the hysteresis increased by over three times. The observed differences are likely due to the fact that the specimen from 5.0 m has some large-size pores (>400 μm), which were not found in specimens from 1.0 and 3.0 m. These large-size pores enhance pore nonuniformity, leading to larger hysteresis and smaller desorption/adsorption rates.

When the vertical net stress was increased from 0 to 50 kPa, the specimens from all depths showed a reduction of hysteresis. Furthermore, the reduction is the most obvious for the specimen from 5.0 m due to the collapse of its large-size pores.

Data Availability

Data are available from the corresponding author upon reasonable request.

Conflicts of Interest

The authors declare that they have no conflicts of interest.

References

[1] J. Muñoz-Castelblanco, P. Delage, J. M. Pereira, and Y. J. Cui, "Some aspects of the compression and collapse behaviour of an unsaturated natural loess," *Géotechnique Letters*, vol. 1, no. 2, pp. 17–22, 2011.

[2] Q. Y. Mu, C. Zhou, and C. W. W. Ng, "Compression and wetting induced volumetric behavior of loess: micro- and macro-investigations," *Transportation Geotechnics*, vol. 23, Article ID 100345, 2020.

[3] Q. Y. Mu, H. Dong, H. J. Liao, C. Zhou, S. B. Li, and J. W. Zhang, "Effects of in situ wetting–drying cycles on the mechanical behaviour of an intact loess," *Canadian Geotechnical Journal*, vol. 59, no. 7, pp. 1281–1284, 2022.

[4] L.-T. Zhan, G.-Y. Li, W.-G. Jiao, T. Wu, J.-W. Lan, and Y.-M. Chen, "Field measurements of water storage capacity in a loess-gravel capillary barrier cover using rainfall simulation tests," *Canadian Geotechnical Journal*, vol. 54, no. 11, pp. 1523–1536, 2017.

[5] Q. Wang, S. Fei, L. Wang, A. Bouazza, S. Shen, and H. Xie, "Investigation of methane fluxes from temporary cover of Xi'an Jiangcungou landfill, China," *Environmental Geotechnics*, vol. 10, no. 4, pp. 241–251, 2023.

[6] G. Li, L. Zhan, S. Zhang, S. Feng, and Z. Zhang, "A dual-porosity model for coupled rainwater and landfill gas transport through capillary barrier covers," *Computers and Geotechnics*, vol. 151, Article ID 104966, 2022.

[7] P. Li, T. Li, and S. K. Vanapalli, "Influence of environmental factors on the wetting front depth: a case study in the Loess Plateau," *Engineering Geology*, vol. 214, pp. 1–10, 2016.

[8] X. Hou, S. K. Vanapalli, and T. Li, "Water infiltration characteristics in loess associated with irrigation activities and its influence on the slope stability in *Heifangtai* loess highland, China," *Engineering Geology*, vol. 234, pp. 27–37, 2018.

[9] J. Muñoz-Castelblanco, J. M. Pereira, P. Delage, and Y. J. Cui, "The water retention properties of a natural unsaturated loess from northern France," *Géotechnique*, vol. 62, no. 2, pp. 95–106, 2012.

[10] C. W. W. Ng, H. Sadeghi, S. K. B. Hossen, C. F. Chiu, E. E. Alonso, and S. Baghbanrezvan, "Water retention and volumetric characteristics of intact and re-compacted loess," *Canadian Geotechnical Journal*, vol. 53, no. 8, pp. 1258–1269, 2016.

[11] Q. Y. Mu, H. Dong, H. J. Liao, Y. J. Dang, and C. Zhou, "Water-retention curves of loess under wetting–drying cycles," *Géotechnique Letters*, vol. 10, no. 2, pp. 135–140, 2020.

[12] P. H. Simms and E. K. Yanful, "Predicting soil-water characteristic curves of compacted plastic soils from measured pore-size distributions," *Géotechnique*, vol. 52, no. 4, pp. 269–278, 2002.

[13] E. Romero, G. Della Vecchia, and C. Jommi, "An insight into the water retention properties of compacted clayey soils," *Géotechnique*, vol. 61, no. 4, pp. 313–328, 2011.

[14] A. Seiphoori, A. Ferrari, and L. Laloui, "Water retention behaviour and microstructural evolution of MX-80 bentonite during wetting and drying cycles," *Géotechnique*, vol. 64, no. 9, pp. 721–734, 2014.

[15] C. W. W. Ng and Y. W. Pang, "Influence of stress state on soil–water characteristics and slope stability," *Journal of Geotechnical and Geoenvironmental Engineering*, vol. 126, no. 2, pp. 157–166, 2000.

[16] ASTM, *Standard D422-63: Standard Test Method for Particle-Size Analysis of Soils*, ASTM International, West Conshohocken, 2007.

[17] ASTM D4318-10, *Test Methods for Liquid Limit, Plastic Limit, and Plasticity Index of Soils. Annnual Book of ASTM Standards*, ASTM International, West Conshohocken, 2010.

[18] Z. Liu, F. Liu, F. Ma et al., "Collapsibility, composition, and microstructure of loess in China," *Canadian Geotechnical Journal*, vol. 53, no. 4, pp. 673–686, 2016.

[19] G. Curioni, D. N. Chapman, A. C. D. Royal et al., "Time domain reflectometry (TDR) potential for soil condition monitoring of geotechnical assets," *Canadian Geotechnical Journal*, vol. 56, no. 7, pp. 942–955, 2019.

[20] Q. Y. Mu, L. T. Zhan, C. P. Lin, and Y. M. Chen, "Non-invasive time domain reflectometry probe for transient measurement of water retention curves in structured soils," *Engineering Geology*, vol. 264, Article ID 105335, 2020.

[21] D. G. Fredlund and H. Rahardjo, *Soil Mechanics for Unsaturated Soils*, John Wiley & Sons, Inc., New York, N.Y., 1993.

[22] G. Zhang, J. T. Germaine, R. Torrence Martin, and A. J. Whittle, "A simple sample-mounting method for random powder X-ray diffraction," *Clays and Clay Minerals*, vol. 51, pp. 218–225, 2003.

[23] P. Delage, M. Audiguier, Y.-J. Cui, and M. D. Howat, "Microstructure of a compacted silt," *Canadian Geotechnical Journal*, vol. 33, no. 1, pp. 150–158, 1996.

[24] V. Sivakumar, *A critical state framework for unsaturated soils*, Ph.D. thesis, University of Sheffield, 1993.

[25] E. Romero and P. H. Simms, "Microstructure investigation in unsaturated soils: a review with special attention to contribution of mercury intrusion porosimetry and environmental scanning electron microscopy," *Geotechnical and Geological Engineering*, vol. 26, pp. 705–727, 2008.

[26] M. T. van Genuchten, "A closed-form equation for predicting the hydraulic conductivity of unsaturated soils," *Soil Science Society of America Journal*, vol. 44, no. 5, pp. 892–898, 1980.

[27] D. G. Fredlund and A. Xing, "Equations for the soil–water characteristic curve," *Canadian Geotechnical Journal*, vol. 31, no. 4, pp. 521–532, 1994.

[28] N. Lu and M. Khorshidi, "Mechanisms for soil-water retention and hysteresis at high suction range," *Journal of Geotechnical and Geoenvironmental Engineering*, vol. 141, no. 8, Article ID 04015032, 2015.